Supplementary Materials

S1. Further details of U-Th measurements, and methods of U-Th dating of materials from 1996 piston core

Samples from the PLJ-1 core were processed from March 2016 to July 2019. As mentioned in the main text, sample powders were spiked with a ^{229}Th-^{233}U-^{236}U isotope tracer. The tracer was made in-house by mixing an IRMM-3636a reference solution (a 1:1 ^{233}U-^{236}U double spike) with a ^{229}Th solution purified from ^{233}U by Aaron Pietruszka (Univ. of Hawaii at Manoa). The isotopic composition of this tracer was then calibrated by combining it with a U-Th gravimetric standard prepared from the New Brunswick Laboratories CRM 112-A uranium metal isotopic standard and an Ames Laboratory thorium metal bar, and then measuring the ^{238}U/^{236}U and ^{232}Th/^{229}Th in the resulting mixed solution.

Replicate analyses from the PLJ-1 core were processed in 21 batches. Powders were dissolved in Teflon beakers cleaned via a boiling-washing procedure with concentrated HNO_3, HCl, and aqua regia. Total procedural blanks were included in each chemistry set and were, on average, 0.13 $\pm$ 0.28 fg ^{230}Th, 5.6 $\pm$ 7.8 pg ^{232}Th, 0.48 $\pm$ 0.91 fg ^{234}U, and 7.6 $\pm$ 8.3 pg ^{238}U. The large standard deviations reflect the impact of $\sim$5 batches for which high blanks were observed. For added context, the median values for the procedural blanks was 0.04 fg ^{230}Th, 2.4 ^{232}Th, 0.09 fg ^{234}U, and 4.0 pg ^{238}U. All analyses were corrected for the contribution from procedural blanks.

On the Nu Plasma II-ES multi-collector ICP-MS at MIT, uranium solutions ranging from 5–40 ppb in concentration and thorium solutions ranging <1–30 ppb in concentration were measured separately. For uranium, the intensities of ^{238}U, ^{236}U, ^{235}U, and ^{233}U were measured on Faraday detectors while ^{234}U was measured on the Secondary Electron Multiplier (SEM) detector. For thorium, ^{232}Th and ^{229}Th were measured on Faraday detectors and ^{230}Th on the SEM detector. The Faraday cup measuring ^{233}U and ^{229}Th had a 10^{12} Ohm resistor in order to measure beam intensities as low as 5 mV without compromising the signal-to-noise ratio.

In addition to being corrected for mass bias and variable SEM yield via bracketing uranium and thorium standards, reported ratios were also corrected for instrument background by measuring 2% HNO_3 solution blanks bracketing each sample and standard analysis. Reported ratios were also corrected for dead time on the ion counter and peak tailing from ^{238}U, ^{236}U, ^{235}U, and ^{232}Th. We also correct for uranium hydride interference with ^{234}U (^{233}U-H$^+$). To date, we have not observed a relationship between mass bias or ion counter gain with signal intensity on this instrument. Measured isotope ratios were also corrected for analyte isotopes contributed by the spike. The uncertainties associated with all these corrections are included in the reported uncertainties.

In October 2016, four aliquots of the GC-1 secular equilibrium standard from Cheng et al. (2013) were prepared and analyzed at MIT applying the same methods as those described in this work. The results gave a mean ^{230}Th/^{238}U activity ratio of 1.001 $\pm$ 0.002 and a mean ^{234}U/^{238}U activity ratio of 1.0000 $\pm$ 0.0008.

U-Th measurements on materials from the 1996 core were performed at the University of Minnesota. For the first set of samples, processed in approximately 1999, mollusc shell fragments were removed prior to chemical processing. For the second set processed in 2011, mollusc shell fragments were not comprehensively removed. Sample preparation was identical to the procedures described in Section 3.2. Samples for the first set were analyzed on a Finnigan Element I using methods described in Shen et al. (2002). Samples for the second set were analyzed using a ThermoScientific Neptune multi-collector ICP-MS in peak-jumping mode using methods described in Shen et al.

(2012) and Cheng et al. (2013).

S2. Methods of other datasets used to interpret U-Th data

Elemental concentration data. We measured 55 sediment samples for elemental concentrations of Ca, Mg, Sr, Al, Ti, P, V, Mn, and Fe. Samples of ∼1–2 mg in weight were dissolved and diluted in 3% HNO_3 and then measured on an Agilent 7900 ICP-MS at the MIT Center for Environmental and Health Sciences. Sample analyses were bracketed by a multi-element standard. Two measurements each were also made on two certified multi-element reference standards, PACS-2 and BCR-2. Data were corrected for blank intensities. Uncertainties for each element were determined by calculating the average percent difference between recommended values and measured values in PACS-2 and BCR-2, and then applying the larger percent difference on measured sample values. For example, the average percent difference between measured and recommended values in Mg (wt %) was 6% for PACS-2 and 2% for BCR-2; thus, all Mg measurements for samples were assigned an uncertainty of 6% of the measured Mg value. Of the 55 samples analyzed, 48 corresponded to U-Th analyses.

Total Inorganic Carbon/Total Organic Carbon. We measured weight percentage total carbon (TC) and weight percentage total inorganic carbon (TIC) by coulometry. For the measurement of TC, we combusted samples at 1000°C using a UIC 5200 automated furnace, and analyzed the resultant CO_2 by coulometry using a UIC 5014 coulometer. Similarly, we measured TIC by acidifying samples with 10% H_3PO_4 using an Automate acidification module and measured the resultant CO_2 by coulometry. We calculated weight percentage total organic carbon (TOC) from TOC = TC–TIC; weight percentage TIC was converted to percent calcite based on stoichiometry.

Color reflectance spectrophotometry. Color reflectance data were measured using a Geotek multi-sensor automated core logger (MSCL-XYZ) on split core sections at LacCore. To calculate sediment optical lightness, we took the sum total of light in the visible region of the electromagnetic spectrum, between 400 and 700 nm, following Balsam et al. (1999).

Mineralogy. In order to characterize the carbonate mineralogy of the drill core and to discern possible mineralogical differences between endogenic and detrital $CaCO_3$, 25 samples were selected from intervals with variable $CaCO_3$ abundance (0–85%) from throughout the core. In addition, 6 samples of carbonate bedrock from within the Junín drainage basin on both the eastern and western sides of the lake were also analyzed. All samples were pretreated with 35% H_2O_2 and 1M NaOH to remove organic matter and biogenic silica, respectively. Samples were then disaggregated with a solution of NaO_3P combined with ultrasonication, and then washed through 53 and 25 µm sieves to isolate fractions >53 µm, 25–53 µm, and, <25 µm. These fractions were then scanned on a Phillips PW 1840 diffractometer at 45 kW and 35 mA. Each subsample was scanned twice, wide scans were conducted at 0.6° (2Θ) per minute from 4.0–70° (2Θ) whereas narrow, more focused, scans were performed at 0.3° per minute from 28.0–31.0°.

Ostracode assemblage analysis. A total of 22 sediment samples corresponding to U-Th analyses were selected for ostracode analysis. One 0.25-g aliquot per sample was removed for most ostracode analyses. Prior to sieving, samples were gently disaggregated with three freeze/thaw cycles, since sediments were densely compacted. Then, samples were wet-sieved using a 63 µm sieve. Ostracodes were extracted with fine brushes, identified and enumerated with respect to numbers per 0.25 g dry sediment. Analysis was done using a Leica M80 stereo-microscope. Adult and juvenile intact and broken valves were differentiated. Broken valves were counted if >50% was encountered and when identification was still possible. Fossil ostracodes were identified down to

family level following procedures described in Pérez et al. (2010) and Karanovic (2012).

Additionally, we made a brief sediment description that included information of other fauna, vegetation and minerals found in the observed sediment samples.

We calculated different ratios to facilitate taphonomy interpretations and for a better understanding of processes such as remineralization and reworking in samples. The broken:intact (B:I) ratio was calculated for each sample to identify samples with relatively high numbers of broken shells. Similarly the adult:juvenile (A:I) ratio was used to identify samples with a high number of adult valves, that could indicate transportation of the lighter juvenile valves to deeper waters. The nektobenthic:benthic (NB:B) was calculated to evaluate shifts in the relative abundance of bottom-swimming versus bottom-dwelling individuals.

Shell coloration was taken into account as well when enumerating ostracode shells. We were able to distinguish 7 different shell colorations: 1. Translucent, 2. White, 3. Partly light grey, 4. Completely light grey, 5. Partly dark grey, 6. Completely dark grey, 7. Completely black. Additionally, we used a Scanning Electron Microscope (SEM) TM3000 Hitachi with BSE Detector II for taking pictures of uncoated specimens to facilitate ostracode identification and to detect elements of ostracode shells using EDX analysis. All ostracode analyses were conducted at the Institut für Geosysteme und Bioindikation (IGeo) of TU-Braunschweig.

S3. Calculation of $\delta^{234}U_{iec}$

Here we derive our formula for calculating the $\delta^{234}U$ of the initial endogenic carbonate ($\delta^{234}U_{iec}$) for a given bulk sediment sample. We make this calculation in order to account for the amount of initial detrital ^{234}U included in our samples. Our calculations assume that each sample is a mixture of two isotopically homogeneous sources—endogenic carbonate and detritus—and that the detrital component has a $^{232}Th/^{238}U$ activity ratio equivalent to the average value of the upper continental crust ($[^{232}Th/^{238}U]_{det} = 1.2 \pm 0.6$) and isotope ratios in the ^{238}U decay chain that are at secular equilibrium ($[^{234}U/^{238}U]_{det} = [^{230}Th/^{238}U]_{det} = 1.0 \pm 0.5$). The uncertainties are set to a conservative $\pm 50\%$ to account for variability and unknown unknowns, following Dutton et al. (2017).

The initial uranium isotopic composition of a sample is defined as follows:

$$\left[\frac{^{234}U}{^{238}U}\right]_{initial} = \left[\frac{^{234}U}{^{238}U}\right]_{det} f_{det} + \left[\frac{^{234}U}{^{238}U}\right]_{iec} (1 - f_{det}), \tag{S1}$$

where the subscript *initial* refers to the initial isotope ratio of the sample, f_{det} is the fraction of uranium in the sample that is detrital, and brackets indicate activities. We rearrange Equation S1 and convert to delta notation to solve for $\delta^{234}U_{iec}$:

$$\delta^{234}U_{iec} = \left(\frac{[^{234}U/^{238}U]_{initial} - [^{234}U/^{238}U]_{det} \times f_{det}}{1 - f_{det}} - 1\right) \times 1000. \tag{S2}$$

Here, f_{det} is defined as follows:

$$f_{det} = \frac{^{238}U_{det}}{^{238}U_{samp}}, \tag{S3}$$

where the subscript *samp* refers to the total bulk sample and subscript *det* refers to the detrital component of the bulk sample. The unknown in the above formula is the amount of $^{238}U_{det}$, since

the amount of ^{238}U$_{\text{samp}}$ is a quantity we measure. Because we also measure ^{232}Th$_{\text{samp}}$, we can use these quantities and our assumption for $[^{232}\text{Th}/^{238}\text{U}]_{\text{det}}$ to solve for f_{det}:

$$f_{\text{det}} = [^{232}\text{Th}]_{\text{samp}} \times \frac{1}{[^{232}\text{Th}/^{238}\text{U}]_{\text{det}}} \times [^{238}\text{U}]_{\text{samp}}. \tag{S4}$$

Substituting Equation S4 for f_{det} in Equation S2 and using the assumed isotopic values for the detrital component of the sample, we can solve for δ^{234}U$_{\text{iec}}$.

For the uncertainty of δ^{234}U$_{\text{iec}}$, we propagate the uncertainties on all measured quantities and assumed detrital activity ratios through differentiation:

$$\sigma_{\delta^{234}\text{U}_{\text{iec}}} = \sqrt{\frac{\sigma_c^2(a-b)^2 + \sigma_a^2(c-1)^2 + \sigma_b^2(c-1)^2 c^2}{(c-1)^4}} \times 1000, \tag{S5}$$

where a is $\left[\frac{^{234}\text{U}}{^{238}\text{U}}\right]_{\text{initial}}$, b is $\left[\frac{^{234}\text{U}}{^{238}\text{U}}\right]_{\text{det}}$, c is f_{det}, and σ is the standard deviation of each of the aforementioned quantities. To calculate σ_c, the standard deviation of f_{det}, we propagate uncertainties of the quantities shown in Equation S4.

S4. Failure to build isochrons

As mentioned in Section 4, determining dates from isochron plots failed, with high MSWDs and probabilities of fit that are close to 0% (Fig. S3). We used the Isoplot 4.1 program by Ludwig (2012) to generate isochron plots of various replicate analyses from bulk sample material, as well as analyses from adjacent clean-dirty sample pairs. Isochron plots assume that the detrital component of a sample is isotopically homogeneous. The top left panel in Fig. S3 is an idealized isochron, which shows replicate analyses following a linear trend in ^{230}Th$/^{238}$U-^{232}Th$/^{238}$U activity space (an "Osmond" isochron diagram). If analyses sufficiently contain variable proportions of detritus, the analyses will plot along a range of ^{232}Th$/^{238}$U activity values ordered from detritus-rich to detritus-poor (see varying shades of gray of ellipses in the idealized isochron of Fig. S3). The y-intercept of the line-of-best-fit through the data marks the ^{230}Th$/^{238}$U activity ratio of the detritus-free endogenic carbonate; when this information is combined with the line-of-best-fit through the same data in ^{234}U$/^{238}$U-^{232}Th$/^{238}$U activity space, which reveals the detritus-free δ^{234}U$_{\text{initial}}$ value, we can calculate a U-Th date.

Contrasting the idealized isochron, the other panels in Fig. S3 are examples of five isochron plots of data from the PLJ-1 core. None of these data exhibit linear coherence along a mixing line, even in isochron plots which display data from adjacent clean-dirty sample pairs (see dark- versus light-colored ellipses) to ensure sufficient spread in ^{232}Th$/^{238}$U activity ratios. In these situations of "excess scatter" or "over-dispersion," a common practice is to expand the uncertainties (the size of the ellipses) by a factor of $\sqrt{\text{MSWD}}$ to account for unknown unknowns (e.g., Ludwig, 2003; Vermeesch, 2018). Unfortunately, doing so here does not improve the fit through data in a meaningful way. Thus, the scatter of these data are further evidence of the existence of open system behavior occurring in these sediments.

S5. Parameters and priors used for Bacon age-depth model

We used the following parameters and priors for our Bacon age-depth model: `thickness` = 50 cm; `acc.mean` = 80 yr/cm; `acc.shape` = 2.0; `mem.strength` = 15; and `mem.mean` = 0.8. The

age-depth model was generated by executing the following command:

```
Bacon(core = "PLJ_dates_d234U_50", acc.mean = 80, acc.shape = 2, mem.mean = 0.8,
mem.strength = 15, thick = 50, ssize = 10000, burnin = 2000, suggest = FALSE, depths.file
= TRUE, yr.max = 800000, MaxYr=781000, d.max = 8800);
```

The Baconvergence test was run and yielded a Gelman and Rubin Reduction Factor of 1.031463, which fell below the 1.05 safety threshold and indicates robust mixing of Markov Chain Monte Carlo iterations.

Trachsel and Telford (2017) tested Bacon and showed that the `thickness` parameter (the segment length) had an unpredictable effect on the size of the error envelope. They also found that the impact of different values for `thickness` was dependent on `acc.shape`, the accumulation shape prior. As Blaauw and Christen (2011) did not explicitly make any recommendations for how to choose an appropriate value for `thickness`, Trachsel and Telford (2017) suggested that the length be shorter than the mean distance between dated intervals and to choose a value that allowed for faster model convergence.

As can be seen from Fig. 16, the chronological constraints of the PLJ-1 splice are not equally spaced. The average distance between radiocarbon data in the upper 20 m of the core is 24 cm; when considering all radiometric data (radiocarbon and U-Th), the average spacing is 72 cm.

Thus, we carried out a comparison of age-depth models generated using different lengths for the `thickness` parameter, keeping the accumulation shape prior constant. Fig. S4 shows that while the difference in the mean of the age-depth models does not vary by more than 8 kyr at any point in the record, there are 5–30 kyr differences in the width of the error envelope.

Unfortunately, there is no rule of thumb or other external information that can help us determine which length for the `thickness` parameter is most appropriate. At this point, the decisions for how to generate the age-depth model are, regrettably, more of an art. Thus, we collectively settled on using 50 cm as the length for the `thickness` parameter, for no other reason other than it seeming "reasonable." We encourage others to use the chronological constraints generated in this study and others at Lake Junín to create better age-depth models with improved estimates of uncertainties.
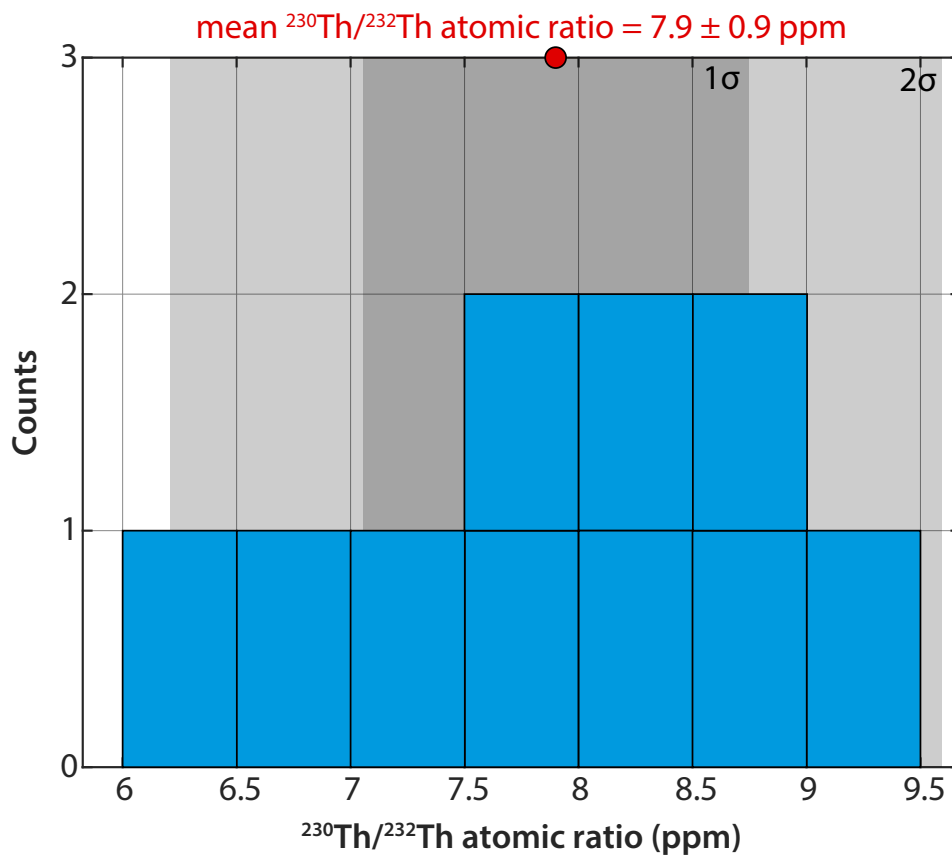
Figure S1: Histogram of ^{230}Th/^{232}Th atomic ratio of indeterminate samples from the 1996 core ($N = 10$). The average ^{230}Th/^{232}Th ratio of these samples is 7.9 $\pm$ 0.9 ppm (1-σ); the mean is represented by the red circle and the one- and two-sigma ranges of these data are represented by the shaded gray areas.
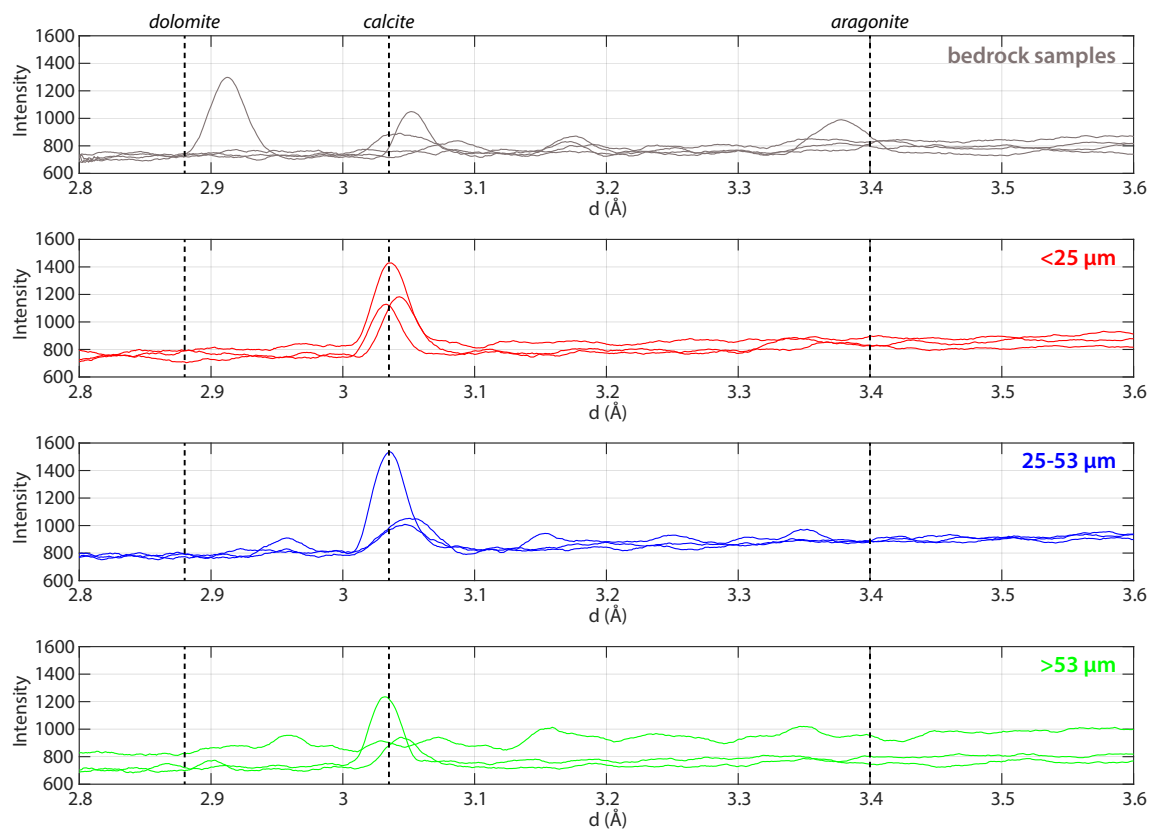
Figure S2: Comparison of XRD spectra between four bedrock carbonate samples collected within the Lake Junín drainage basin (top) and specific grain size fractions of three core catcher samples from high carbonate intervals (>70%) in the PLJ-1 core. The different grain size fractions analyzed were <25 µm, 25–53 µm, and >53 µm. The three core catcher samples plotted here are 1E-15H-3 (∼73 m CCLF), 1D-18H-3 (∼53 m CCLF), and 1D-23H-3 (∼67 m CCLF). The four bedrock samples are from Huarmipuquio (11.167°S, 76.046°W, 4115 masl), Ondors (11.098°S, 76.127°W, 4115 masl), El Mirador (11.057°S, 76.158°W, 4118 masl), and the east side of Lake Junín (10.864°S, 75.987°W, 4470 masl).
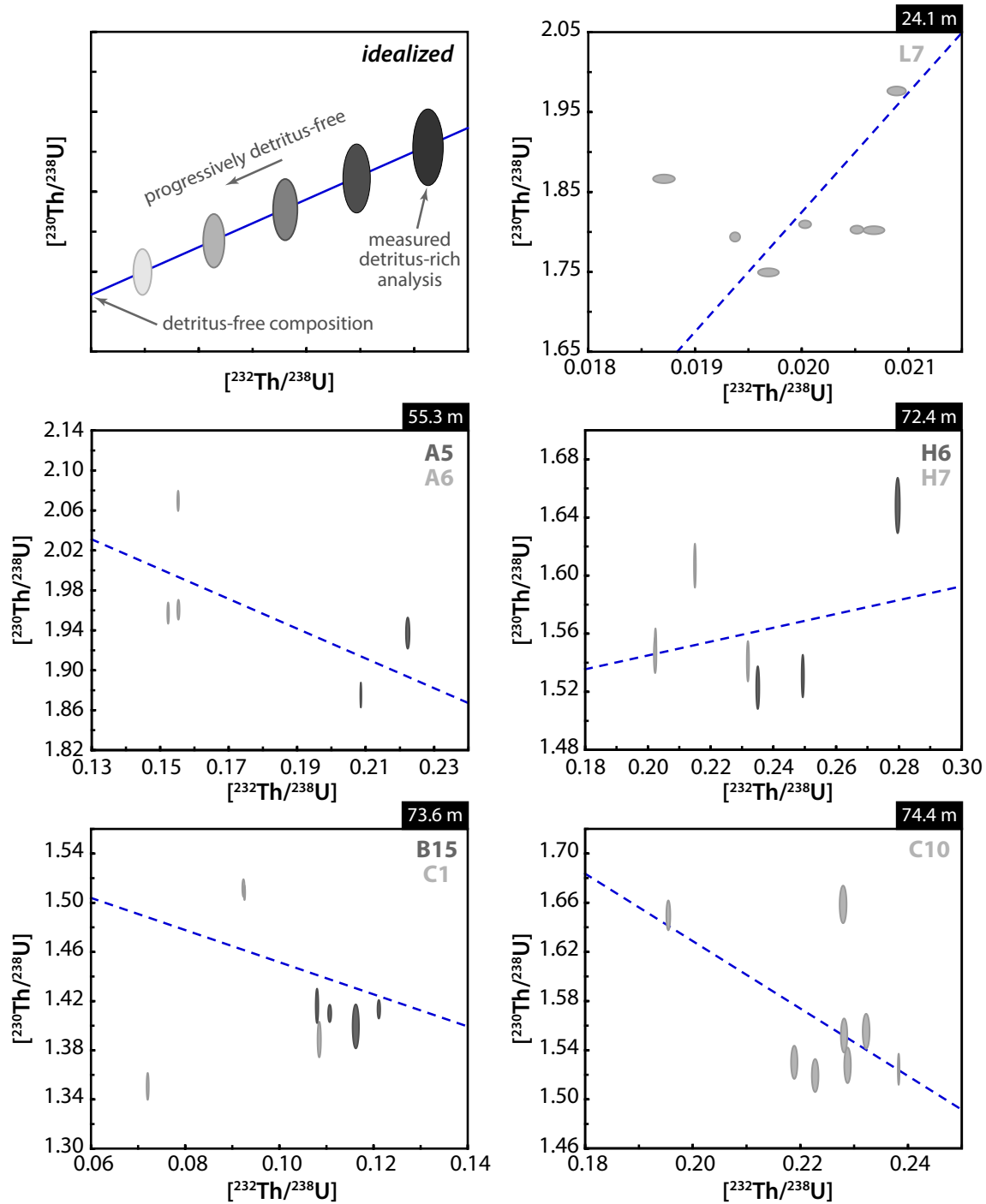
Figure S3: Examples of five isochron diagrams ("Osmond" type) made from replicates of samples from the PLJ-1 core. Each ellipse represents the 2-σ uncertainties of a replicate analysis for activity ratios ^{232}Th/^{238}U and ^{230}Th/^{238}U. Blue dashed lines represent the error-weighted, least-squares regression through shown data. Top left panel shows an idealized version of an isochron plot, in which replicate analyses fall along a regression line with a high probability of fit. In the remaining five panels, the CCLF depth of the analyses is indicated in the black rectangular box, and the corresponding Sample ID is listed in the top right corner. For some plots, replicate analyses from two unique samples are shown; these are instances in which two samples immediately adjacent to one another were collected. For these sample pairs, analyses from the sample that was visually assessed as 'dirtier' are represented by a dark gray ellipse. Isochron diagrams were made using Isoplot 4.1 (Ludwig, 2003).
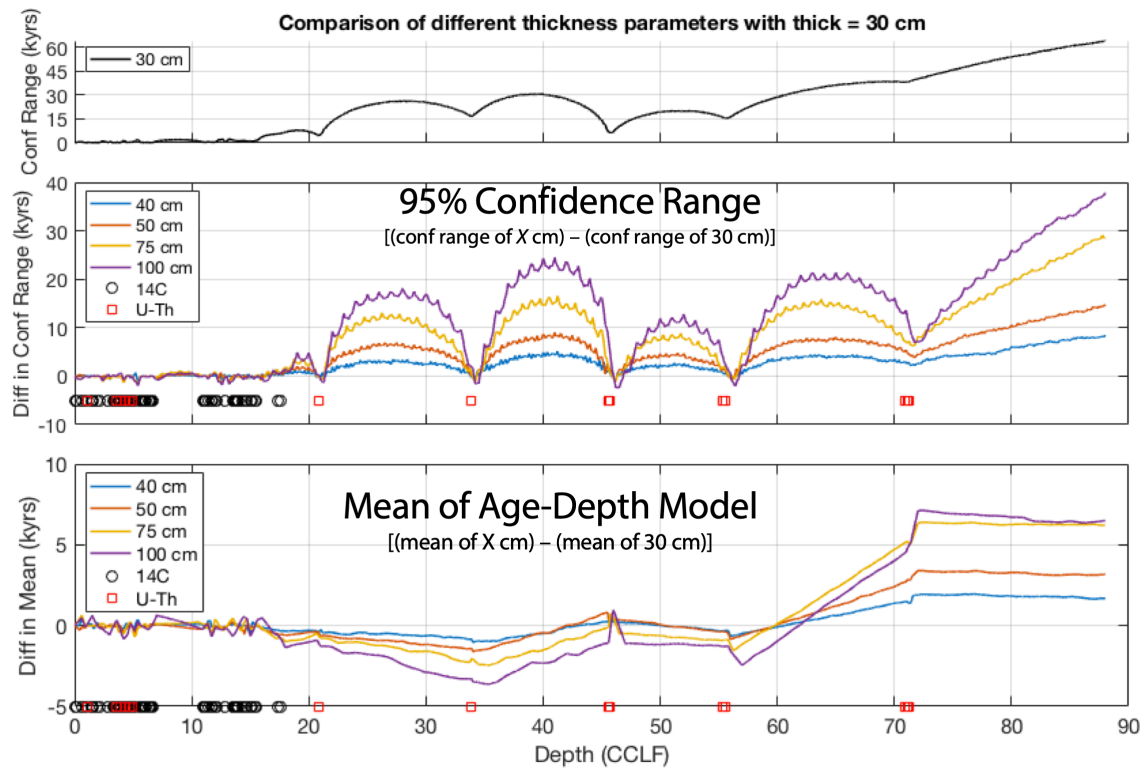
Figure S4: Comparison of the size of the 95% confidence range and mean of Bacon age-depth models run with varying lengths of the `thickness` parameter. Middle and bottom plots compare the age-depth models to the results of the model where `thickness` = 30 cm. The top plot shows the size of the 95% confidence range for the age-depth model where `thickness` = 30 cm.
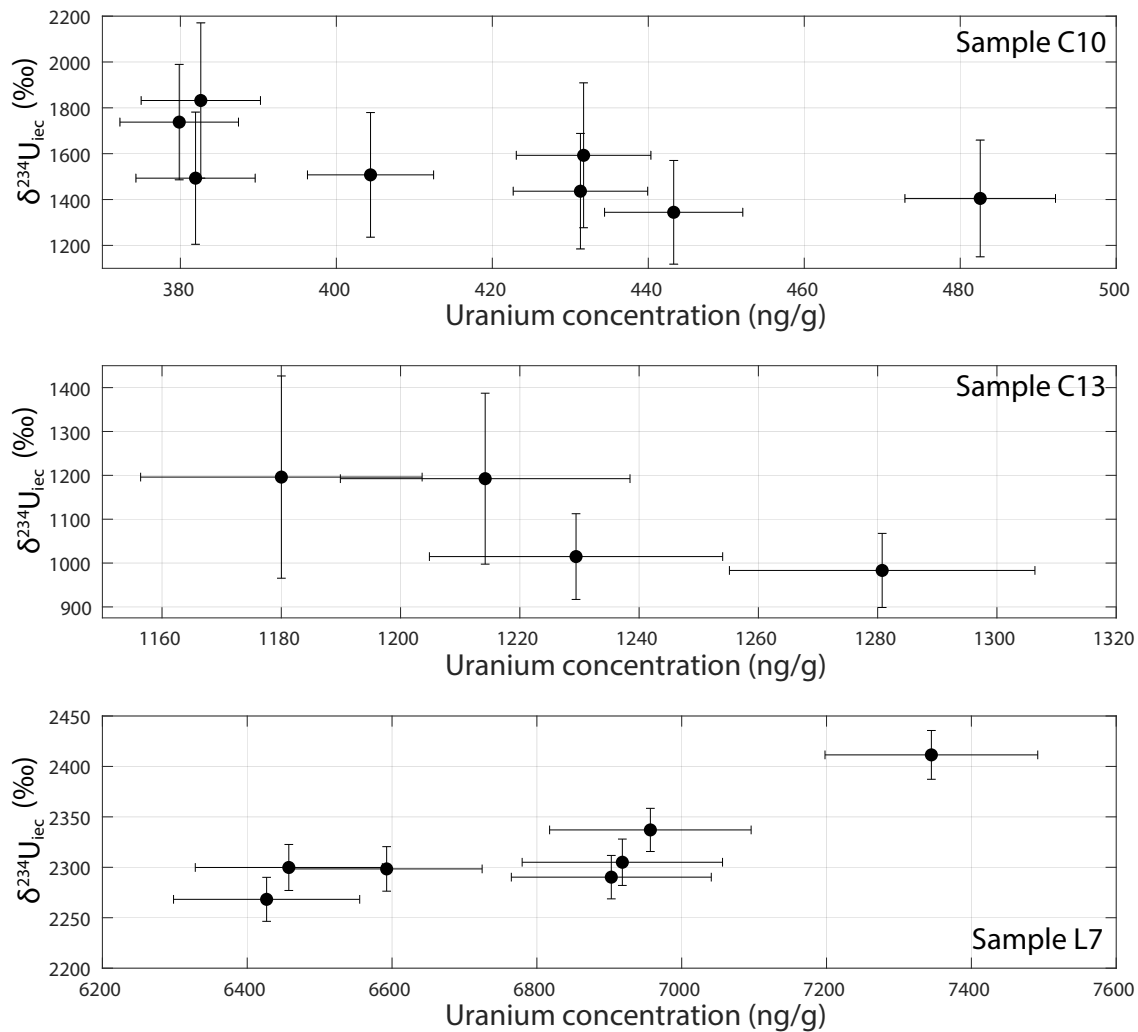
Figure S5: Comparison of uranium concentration and $\delta^{234}U_{iec}$ for three samples of the CMC facies: C10 (top), C13 (middle), and L7 (bottom). Samples C10 and C13 show some evidence of the inverse relationship between uranium concentration and $^{234}U_{iec}$, as would be predicted if there was preferential loss of ^{234}U (Robinson et al., 2006). However, L7—the sample with the highest mean uranium concentrations out of any sample analyzed—does not show a trend that is consistent with the prediction. All errors are at the 2-σ level.